Characteristics of helium DC plasma jets at atmospheric pressure with multiple cathodes*

Cheng Wang(王城)[1,†], Zelong Zhang(张泽龙)[1], Haichao Cui(崔海超)[1], Weiluo Xia(夏维珞)[2], and Weidong Xia(夏维东)[1]

[1] *Department of Thermal Science and Energy Engineering, University of Science and Technology of China, Hefei* 230027, *China*
[2] *Hefei Institutes of Physical Science, Chinese Academy of Sciences, Hefei* 230031, *China*

(Received 17 March 2017; revised manuscript received 16 May 2017; published online 10 July 2017)

A novel DC plasma torch with multiple cathodes is developed for generating laminar, transitional and turbulent plasma jets. The jet's characteristics, including jet appearance, voltage fluctuation, thermal efficiency, specific enthalpy, and distributions of temperature, pressure, and velocity, are experimentally investigated. The results show that as the gas flow rate increases, the plasma jet transforms first from the laminar state to the transitional state and second to the turbulent state. Compared with the transitional/turbulent jet, the laminar jet possesses not only a better stability and a longer high-temperature zone but also a higher average/core temperature and a higher specific enthalpy at the nozzle's outlet. With the change of jet states from the laminar to the turbulent flow, the core pressure and velocity at the nozzle's outlet increase, while the decaying rates of temperature/pressure/velocity along the jet's axial direction increase sharply. Furthermore, applications of laminar, transitional and turbulent jets for zirconia spray coating are described. The test results indicate that the long laminar jet is favorable for the deposition of a high-quality coating because the powder particles injected into the laminar jet may have better heating and lower kinetic energy.

Keywords: arc plasma jet, jet appearance, jet parameters distribution, zirconia coating

PACS: 52.75.Hn, 52.80.Mg, 52.70.–m, 52.77.Fv **DOI:** 10.1088/1674-1056/26/8/085207

1. Introduction

Arc plasma jets at atmospheric pressure have high application value and development potential in industry because of their unique properties such as high temperature, high enthalpy, and high-energy intensity.[1–4] Based on the flow condition, the plasma jet is usually classified as a laminar jet, a transitional jet, or a turbulent jet.[2,5] A long and stable plasma jet with very low noise is defined as running in the laminar state. A short and noisy plasma jet with a significant gas entrainment phenomenon is identified as a turbulent jet. When the laminar and the turbulent jet are converted to each other, the jet length changes rapidly and the resulting flow is classified as a transitional jet.

A large number of studies have indicated that there are distinct differences in the plasma parameters for the laminar, transitional, and turbulent jets, thereby affecting the energy transport and interaction between the plasma jet and the particles immersed in the flow. Pan *et al.*[6–10] conducted a considerable amount of research on the character of the laminar and turbulent jets. Results showed that compared with the turbulent jet, the high-temperature region of the laminar jet possesses not only excellent stability but also a greatly reduced temperature and pressure gradient in the axial direction. By comparing the laminar and the turbulent jet impinging upon a flat plate in ambient air, Wang *et al.*[11–13] determined that a larger amount of air was entrained into the turbulent jet, which increased the decaying rates of the plasma parameters in the turbulent-impinging jet. Thus, the stable laminar jet appears to be more suitable for remelting, hardening, and processing of material surfaces.[8,14–17] Recently, Cao *et al.*[5] investigated the evolution of the appearance of a plasma jet with different gas flows and concluded that the transitional jet had a higher temperature and energy than the laminar jet, which could make the transitional jet better suited for industrial use; however, this concept has not been confirmed with sufficient experiments. In fact, plasma jets applied in the industry are mostly operated in the turbulent state, because the laminar jet is often generated within a relatively narrow range of control parameters and suffers from low thermal efficiency compared to the turbulent jet.[7,18]

In our recent work, a novel DC plasma torch with multiple cathodes was developed.[19–21] Plasma jets including laminar jets, transitional jets, and turbulent jets were examined in the experiment but little work has been conducted on the characteristics of plasma jets. The temperature, pressure, velocity, and fluctuation of the plasma jet are important factors that may affect material processing. In addition, the features of the plasma jet for different torch types are usually quite

*Project supported by the National Natural Science Foundation of China (Grant Nos. 11475174 and 11675177) and the Fundamental Research Funds for the Central Universities, China (Grant No. WK2090130021).

†Corresponding author. E-mail: awcheng@mail.ustc.edu.cn

© 2017 Chinese Physical Society and IOP Publishing Ltd

different;[18,22] therefore, research on plasma jets generated by novel plasma torches is needed.

In this paper, laminar, transitional, and turbulent jets are generated with a novel DC plasma torch with multiple cathodes under different gas flow rates and input power conditions. A preliminary investigation on the new plasma torch is made. Changes in the jet's length and the torch's voltage fluctuation, thermal efficiency, and specific enthalpy are experimentally tested. Temperature, pressure, and velocity of the plasma jets are measured using a homemade water-cooled probe. In addition, the use of plasma jets under different states for the preparation of a zirconia coating is investigated. It is our hope that this paper may provide basic support for using the novel plasma torch in practical applications for material processing.

2. Apparatus and methods

2.1. Experimental apparatus

Figure 1 shows the experimental setup, which is mainly composed of a novel plasma torch, a DC power source unit, a gas supply unit, a cooling unit, a measurement system, and a spray system. The power source unit consists of several independent DC power supplies with a common anode. Each power supply uses an IGBT-based source (200 V, 200 A). The conversion efficiency is more than 90% and the current fluctuation is less than 1%. The gas supply unit provides working gas to the plasma torch accurately by using controllers for the gas flow rate. The measurement system includes a camera and a water-cooled probe. The spray system is composed of a powder delivery device and a stainless steel substrate.

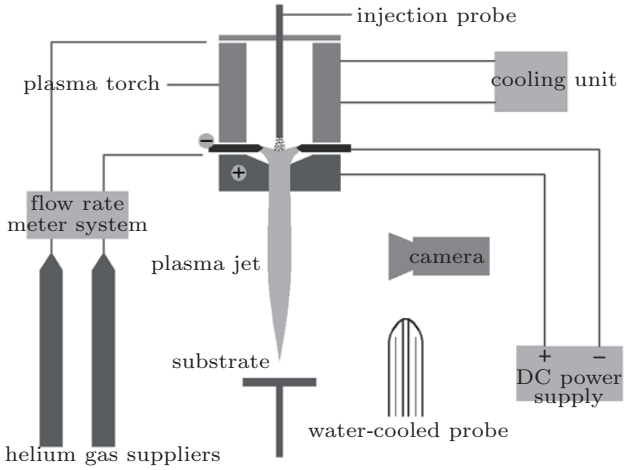


Fig. 1. Schematic diagram of the experimental setup.

A torch with multiple cathodes, principally the same system as described in previous research,[19–21] is used to produce plasma jets at atmospheric pressure. The longitudinal section view of the novel DC arc plasma torch is shown in Fig. 2. The torch is constructed using six multiple tungsten cathodes, a common copper anode, a chamber, and a glass window. An anode nozzle with a backward-facing step is used. The cathode spacing can be adjusted simultaneously allowing the electrode tips to be positioned on a pitch circle varying from approximately 10 mm–40 mm in diameter. The vertical distance from the cathode tips to the anode is about 15 mm. The plasma-forming gas and the window protection gas are introduced separately and their flow ratio is 1:1. Six independent DC power supplies are connected to six cathodes. All components of the plasma torch are directly cooled by the cooling water, so as to decrease the erosion. The arc is ignited using a high-frequency and high-voltage generator.

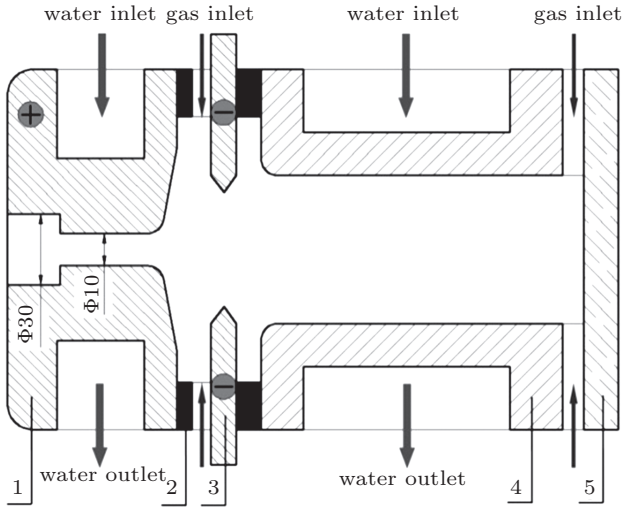


Fig. 2. Schematic diagrams of the plasma torch with multiple cathodes. 1: Anode, 2: insulation piece, 3: cathode, 4: chamber, 5: glass window.

Table 1 shows the range of working conditions. The diameter of the cathode is 5 mm and the diagonal distance between the cathode tips is 30 mm. The internal diameter of the anode nozzle and its backward-facing step is 10 mm and 30 mm respectively and the length is 40 mm and 30 mm respectively. Pure helium gas is used as the working gas at a feeding flow rate of 15 slm–35 slm. The total arc currents of the six cathodes are in the range of 200 A–300 A, and the input power is 10 kW–20 kW.

Table 1. Range of working conditions in this paper.

Arc current/A	200, 250, 300
Input powder/kW	10–20
Plasma forming and protection gas	helium gas
Gas flow rate/slm	15–35
Cathode type	2%-wt lanthanum tungsten cathode, rod type, diameter: 6 mm, tip angle: 60°, cathode number: 6, diagonal distances between cathode tips: 30 mm
Anode type	Red copper, nozzle internal diameter: 10 mm (40 mm length), backward-facing step diameter: 30 mm (30 mm length)

2.2. Measurement system

The arc voltage is recorded with a voltage divider and a 100-kHz wideband data acquisition card. A digital camera (Canon 5D Mark III) is employed to capture the appearance of the plasma jet. The jet length is obtained by measurements from the jet images using a scale.

As shown in Fig. 1, the temperature and mass rate of the cooling water at the outlet and inlet are measured using two thermocouples and a flowmeter respectively, thus the thermal efficiency and the specific enthalpy are calculated by using Eqs. (1) and (2)

$$\eta = (UI - c_p m\Delta T)/UI, \tag{1}$$

$$h = UI\eta/G_{\text{gas}}, \tag{2}$$

where η is the thermal efficiency of the plasma torch, U and I are the arc voltage and the arc current, c_p, m, and ΔT are the specific heat, the mass flow, and the temperature difference of the cooling water respectively, h is the specific enthalpy of the plasma jet, and G_{gas} is the gas mass flow.

A homemade water-cooled probe is employed to measure the core temperature and stagnation pressure of the plasma jet. Figure 3 depicts a schematic diagram of the measuring method. The probe is composed of three copper tubes. The outside surface of the probe is covered with a zirconia ceramic tube to create a thermal insulation layer. The temperature and mass rate of the cooling water at the outlet and inlet, and the temperature and mass rate of the plasma gas at the center hole's outlet are obtained using several thermocouples and flowmeters respectively. The temperature of the plasma jet can be obtained by using Eq. (3).

$$G_{\text{gas}}(h_1 - h_2) = c_p m\Delta T, \tag{3}$$

where G_{gas} is the plasma gas mass flow, h_1 and h_2 are the specific enthalpy of the plasma gas at the probe's inlet and outlet, respectively, and c_p, m, ΔT are the specific heat, the mass flow, and the temperature difference of the cooling water respectively. Based on the specific enthalpy of plasma gas at the probe's inlet, the temperature of the plasma jet can be obtained.

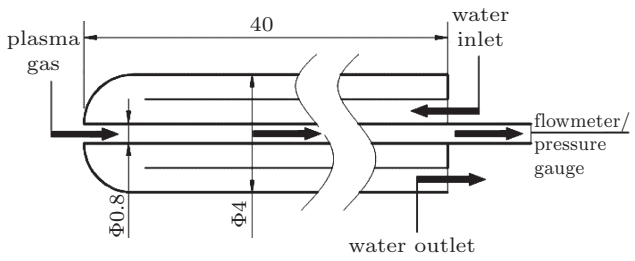


Fig. 3. Schematic diagrams of the water-cooled probe.

The center hole can be used as a pitot tube to measure the velocity of the plasma jet. The stagnation pressure of the plasma jet is measured with a pressure gauge, which is installed at the probe's outlet. The velocity is usually calculated with the following equation.

$$v = \sqrt{2(p - p_0)/\rho}, \tag{4}$$

where v is the velocity of the plasma jet, p and p_0 are the stagnation pressure and static pressure of plasma jet. ρ is the density of the plasma gas at the inlet and is determined by the temperature of plasma jet. In general, p_0 the is equal to one atmospheric pressure.

2.3. Spray system

The schematic diagram of the spray system is shown in Fig. 1. In this study, the experiment adopts the method of using the centeral axis to send the powder because this torch with multiple cathodes provides a proper space for axially-fed feedstock particles. The particles are fed through an injection probe to the arc plasma flame with an appropriate carrier gas. The inner diameter of the injection probe is 4 mm and the probe outlet is located at 5 mm above the plane of the cathode tips. The powder-feeding rate is controlled by a screw-based powder delivery device (PFD402-FM, TEKNA). A stainless steel (1Cr18Ni9Ti) plate with the dimension of $\Phi 15 \times 15$ mm is used as the treated substrate. Prior to spray coating, the substrate is rubbed with sandpaper (280 mesh and 600 mesh), thus increasing the substrate surface roughness, which can help improve the bonding strength of the spray coatings. The microstructure of zirconia coatings is performed on a Sirion 200 apparatus. The detailed working parameters are listed in Table 2.

Table 2. Spraying parameters.

Arc current/A	250
Input powder/kW	10–20
Plasma forming and protection gas	helium gas; gas flow rate: 22.5, 27.5, 32.5 slm
Carrier gas	helium gas; Gas flow rate: 1.0 slm
Zirconia	size: 20–40 μm; particles feeding rate: 5 g/min
Torch-substrate distance/cm	20

3. Results and discussion

3.1. Generation of plasma jets

Figure 4 shows window-viewed images of the cathodes and arc plasma. It is evident that arc discharges take places between six discrete cathodes and a common anode. There do not exist several discrete discharge channels in this experimental range although six independent DC power supplies are respectively connected to each cathode. Between the cathodes and anode nozzle, the arc plasma presents a relatively uniform and stable state, which is referred to as a "diffuse arc".

The characteristics and formation mechanism of the diffuse arc were discussed in Ref. [19]. The diffuse arc converges in the anode nozzle to form a luminous arc column. Within the constraints of anode nozzle and proper gas flow, a long laminar plasma jet can be achieved, as shown in Fig. 5. In our previous research, it was confirmed that gas component, gas flow rate, arc currents and anode nozzle diameter were the main factors affecting the plasma jet's appearances.[21] In the next sections, the influence of gas flow rate and arc currents on the jet's characteristics is investigated.

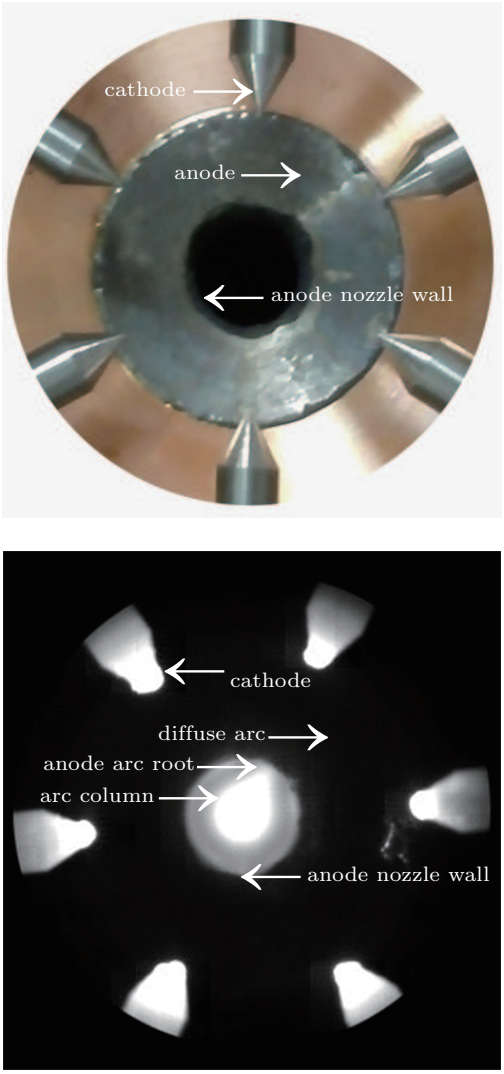


Fig. 4. (color online) Typical window-viewed images of the cathodes and the arc plasma. $I = 250$ A, 25-slm gas flow rate.



Fig. 5. Appearances of the plasma jet. $I = 250$ A, 25-slm gas flow rate.

3.2. Jet appearance

Figure 6 shows the plasma jets' appearance with a gas flow rate from 20 slm to 32.5 slm at $I = 250$ A. Typical arc voltage waves are plotted in Fig. 7. The results indicate that the plasma jet length first increases and then decreases as the gas flow rate increases When the gas flow rate ranges from 20 slm to 25 slm, the plasma jet is operated in the laminar flow with a very low noise. The arc voltage is quite stable, and the voltage fluctuation is less than 4% (2-V fluctuation). The plasma jet length increases with the increase in the gas flow rate, and the maximum length is about 60 cm. With a further increase in the gas flow rate, the plasma jet length is dramatically reduced, while the jet diameter, arc voltage, and voltage fluctuation clearly increase. Based on the significant air entrainment phenomenon at the outer end, it is inferred that the plasma jet is changing from the laminar to the turbulent state. This flow state is usually regarded as a transitional state. When the gas flow rate increases to 32.5 slm, the plasma jet length is reduced to less than 15 cm and a high-intensity noise emission occurs, which indicates the jet is operated in the turbulent state. The arc voltage is nearly 70 V and is accompanied by an enhanced fluctuation (more than 18%, 13-V fluctuation). As the gas flow rate continues to increase, the appearance of the turbulent jet does not change any further.

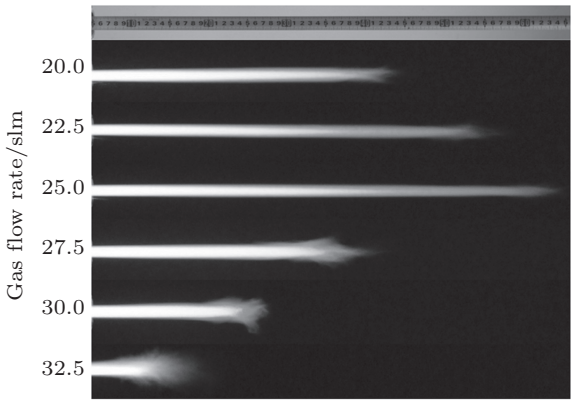


Fig. 6. Appearances of the plasma jets with different gas flow rates. $I = 250$ A.

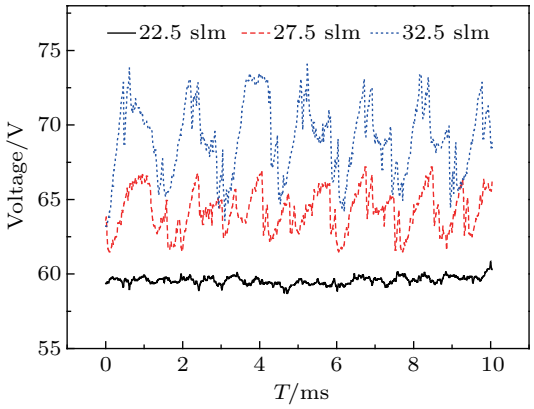


Fig. 7. (color online) Time-resolved arc voltage wave with different gas flow rates, $I = 250$ A.

Figure 8 exhibits the plasma jet length with different gas flow rates and arc currents. It is evident that the jet length has a similar changing trend under different arc currents but

the increasing arc currents are advantageous for improving the jet length and provide a relatively wide range of the gas flow rate for the generation of the long laminar jet. In addition, figure 8 indicates that a critical Reynolds number exists at which the plasma jet transforms from the laminar to the turbulent state. The Reynolds number is directly proportional to the mass flow but inversely proportional to the flow's viscosity. For the plasma jet, the increase in the arc current can result in an increase in gas temperature at a given gas flow rate. Since the viscosity of the helium gas exhibits a monotonically increasing function of temperature during 10000 K–15000 K, higher arc currents should have a greater critical gas flow rate while the critical Reynolds number remains unchanged. The average temperature measured in Subsection 3.3 is used to calculate the Reynolds number. The estimated critical Reynolds number is about 25, which is much lower than the one operated in argon ambient gas.[10] However, using the Reynolds number calculated in a conventional manner may not be a sufficient criterion for flow transition in this study because the plasma flow is relatively complicated. Factors such as the transport coefficient of the working gas, arc root behaviors, and torch structure can strongly affect the jet's appearance.[10] Thus, the critical Reynolds number shown in this paper may be only suitable for a range of the testing parameters.

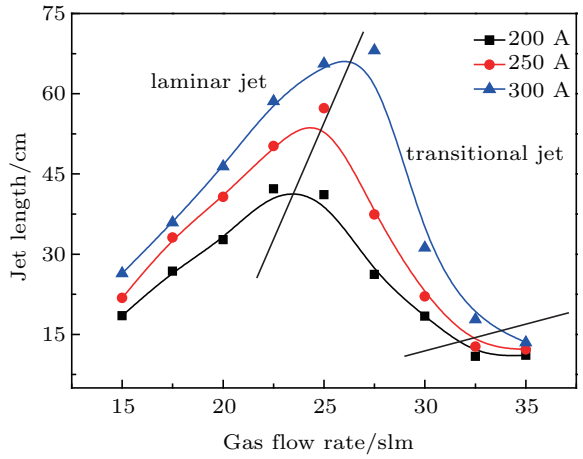


Fig. 8. (color online) Variation of the plasma jet flow state and jet length with different gas flow rates and arc currents.

3.3. Thermal efficiency and specific enthalpy

Figures 9 and 10 show that both arc voltage/arc power and thermal efficiency increase monotonically with the increase in the gas flow rate but decrease with the increase in the arc currents. Although the plasma jets' appearance displays a dramatic change when the jet flow transforms from the laminar flow to the turbulent flow, the arc voltage and thermal efficiency retain a smooth change trend. The maximum thermal efficiency can approach 50% while the minimum value is less than 25%. The torch's thermal efficiency is close to the efficiency of multi-electrode plasma torches with a segmented anode structure[7,18,23] but lower than the efficiency of conventional two-electrode plasma torches without any inter-electrode inserts.[22] In our opinion, the torch construction is the main factor affecting the thermal efficiency. As described in previous research,[19–21] due to the existence of multiple cathodes, the arc plasma between the electrodes appears as a large area diffuse state, which would enhance the heat transfer from the arc plasma to the anode's inner surface. Thus, the thermal efficiency is not sufficiently high.

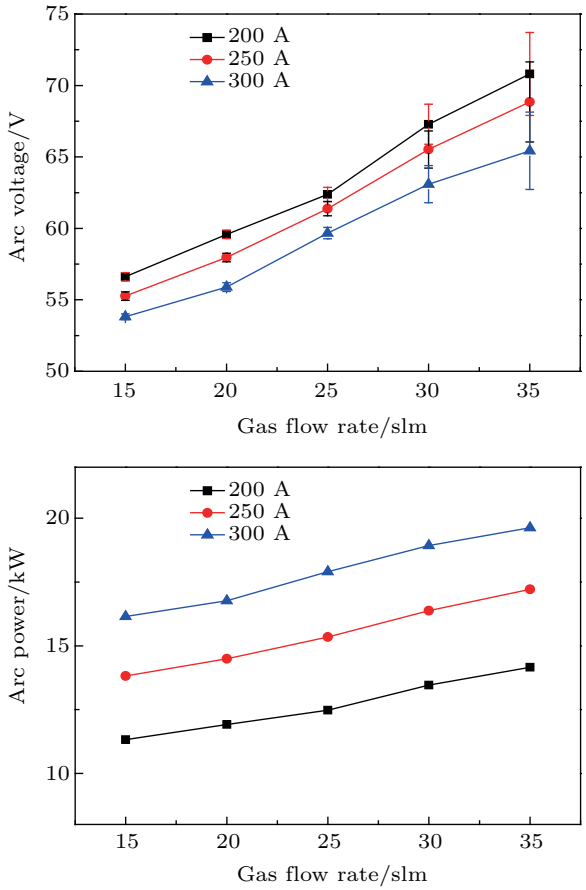


Fig. 9. (color online) Variation of the arc voltage and arc power with different gas flow rates and arc currents.

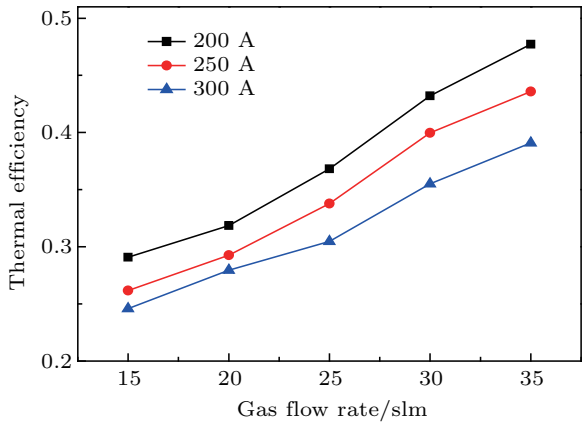


Fig. 10. (color online) Variation of the thermal efficiency with different gas flow rates and arc currents.

The specific enthalpy of the plasma jet at different working parameters is shown in Fig. 11. The specific enthalpy in-

creases with the increase in the arc currents but decreases with the rise of the gas flow rate. This variation can be ascribed to two factors. Firstly, the rise of arc currents increases the gas temperature of the plasma jet, so that the specific enthalpy is improved. Secondly, the total enthalpy of the plasma jet increases with the increase in the gas flow rate because of the increasing arc power and thermal efficiency. However, the increasing gas flow rate surpasses the effect of the total enthalpy on the specific enthalpy. Based on Eqs. (2), the specific enthalpy is negatively correlated with the gas flow rate. The changing trend of the specific enthalpy with changes in the gas flow rate is somewhat different from the results described in previous research.[7,22] This difference is mainly related to the type of working gas and the torch's structure.

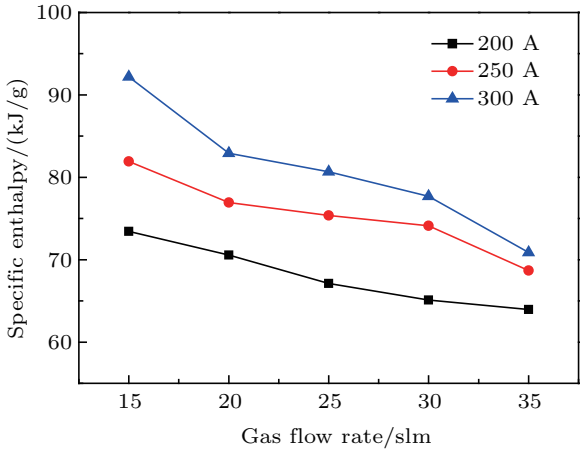


Fig. 11. (color online) Variation of the specific enthalpy with different gas flow rates and arc currents.

3.4. Temperature, pressure, and velocity

The average temperature and core temperature at the nozzle's outlet are plotted in Fig. 12. To lessen the effect of the probe on the plasma jet, the measurement point is just 5 mm in front of the nozzle's outlet. The average temperature is obtained from the specific enthalpy, and the core temperature is calculated by using Eq. (3). Both types of temperatures exhibit an increase with the increase of the arc currents. The core temperature increases from 16730 K at $I = 200$ A to 19330 K at $I = 300$ A with a 15-slm gas flow rate. In accordance with the changing trend of specific enthalpy, the average temperature and core temperature decrease gradually with the rise of the gas flow rate. For example, with $I = 250$ A, the core temperature decreases from 17910 K to 16020 K as the gas flow rate increases from 15 slm to 35 slm.

Figure 13 shows the average velocity and core velocity of the plasma jet at the nozzle's outlet. The average velocity is estimated by the average gas density and gas flow rate, and the core velocity is obtained by Eq. (4). The results indicate that both the average velocity and the core velocity increase with the rise of the gas flow rate and the arc currents, although the temperature descends with the increase in the gas flow rate. The maximum core velocity in the range of experiments is 1300 m/s (about March 0.2). The growth of the inlet velocity is the main driving force that causes the increase in the jet's velocity.

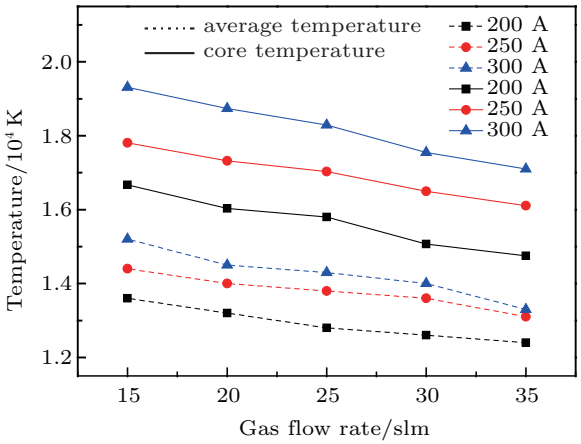


Fig. 12. (color online) Plasma jet's temperature at the nozzle's outlet with different gas flow rates and arc currents.

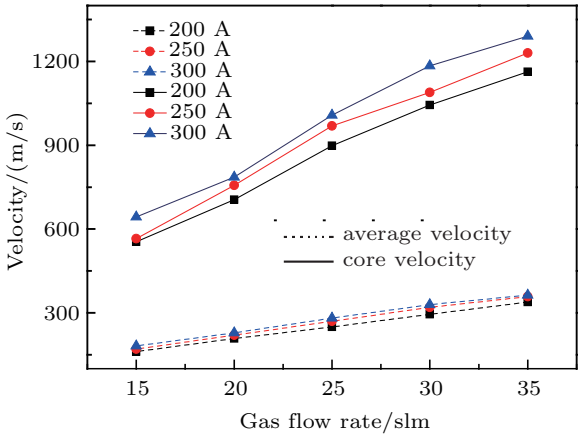


Fig. 13. (color online) Plasma jet's velocity at the nozzle's outlet with different gas flow rates and arc currents.

Figures 14–16 show the distribution of temperature, gage pressure, and core velocity along the jet axial direction under different jet states for the plasma jets. Figure 14 indicates all the temperatures have a clear downward trend along the axial directions, but the declining rate is clearly different. For the laminar jet, the temperature gradient is about 60 K/mm; for the transitional jet, the temperature gradient is nearly 90 K/mm and the temperature gradient is more than 110 K/mm for the turbulent jet. The gage pressure and core velocity also decrease with the increase in axial distance, as exhibited in Figs. 15 and 16. It is found that the gage pressure and core velocity are much lower for the laminar jet than for the transitional/turbulent jet at the nozzle outlet. With the change of jet states from the laminar flow to the turbulent flow, the decaying rates of gage pressure and velocity increase sharply. At 85 mm, the core velocity of the transitional and turbulent jets is even lower than for the laminar jet. Compared

with the laminar jet, more intensive air entrainment occurring in the transitional/turbulent jet because of the enhanced turbulence intensity. The energy dissipation of plasma jet increases rapidly, which can result in a fast attenuation of jet velocity and gage pressure.

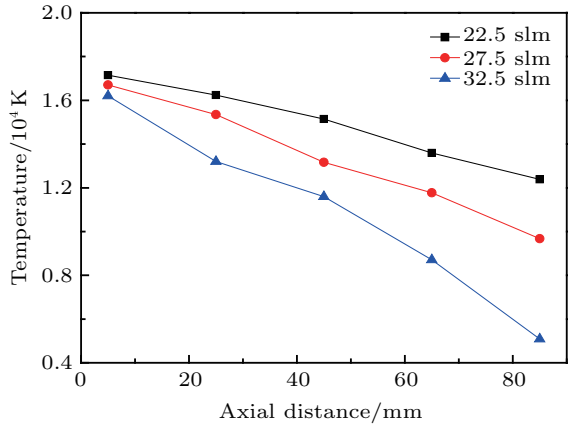


Fig. 14. (color online) Plasma jet's temperature distribution along axial direction. $I = 250$ A.

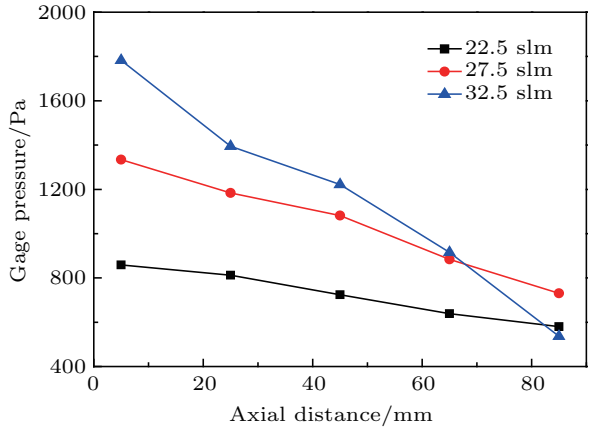


Fig. 15. (color online) Plasma jet's gage pressure distribution along axial direction. $I = 250$ A.

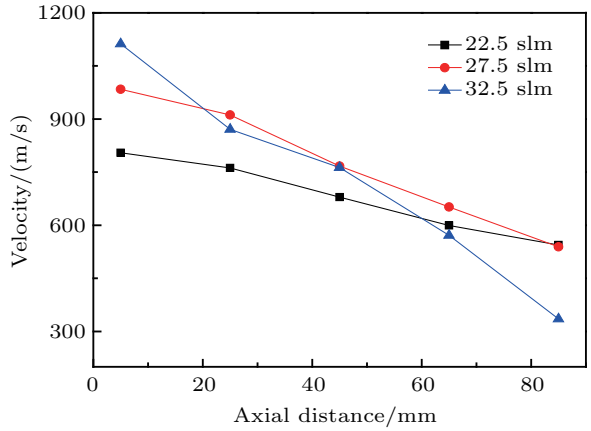


Fig. 16. (color online) Plasma jet's core velocity distribution along axial direction. $I = 250$ A.

3.5. Preparation of zirconia coating

As mentioned above, the laminar, transitional, and turbulent jets have their own special features, which are mainly embodied in the torch's thermal efficiency, plasma jet's stability, length, temperature, etc. These characteristics have great influence on the energy transfer and interaction between the plasma jet and the particles, thus affecting the controllability of the process when the plasma jet is used for spraying. In this section, applications of the torch for the preparation of zirconia coating are tested under different conditions of jet flow. The arc currents are 250 A and the gas flow rate is in the range of 22.5 slm–32.5 slm, so that the plasma jet can be operated in the laminar, transitional, and turbulent state respectively. It is necessary to state that because the powder particles are injected directly into the arc area, the appearance of plasma jet is affected negatively, as shown in Fig. 17. Compared with the plasma jet without powder injection (Fig. 6), the length of plasma jet with powder injection is shorter. However, the steady state of laminar plasma jet can be kept in the experimental conditions presented in Fig. 17.

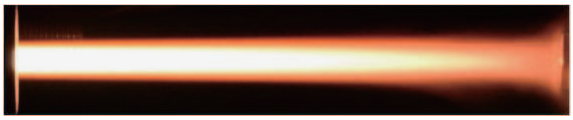


Fig. 17. (color online) Typical appearance of the plasma jet with powder-feeding rate of 5 g/min. $I = 250$ A, 22.5 slm gas flow rate.

Figure 18 gives the scanning electron microscope (SEM) surface views of zirconia coatings prepared using the laminar, transitional, and turbulent jets respectively. It is evident that the overall uniformity of the coating is better when sprayed with the laminar jet than with the transitional or turbulent jet. An evident feature of the coatings is that more discrete and small particles are attached to the coating's surface with the change of jet states from the laminar flow to the turbulent flow. Figure 18(a) shows that the zirconia particles have been completely melted for the plasma spraying using the laminar jet. The coating's surface is rather smooth. For the transitional jet, several strip-shape particles appear on the coating's surface as exhibited in Fig. 18(b), which indicates a splashing phenomenon occurs when the particle droplets impact the substrate. For the turbulent jet, both the splashing structure and some partially molten powder particles exist on the coating's surface, as indicated by the arrows in Fig. 18(c).

In general, the impact velocity of the droplets and the molten state of the ceramic powder particles on the substrate are the key factors that affect the properties of the coating.[24] As described in Subsections 3.2–3.4, the temperature of the laminar jet is higher than that of the transitional and turbulent jets. In addition, the long laminar jet provides sufficient residence time for the particles in the plasma plumes. Therefore, a more efficient energy transfer occurs between the plasma jet and the powder particles, which is beneficial for the melting

of the powder particles. Moreover, because of the small velocity of the laminar jet, the particles injected into the laminar jet have a lower kinetic energy than those in the transitional and turbulent jets. The lower kinetic energy can limit splashing of the particle droplets. This explains the increased splashing phenomenon that occurs with the transitional and turbulent jets. Thus, the characteristics of the long laminar jet may be favorable for the deposition of a highquality coating during the spraying procedure.

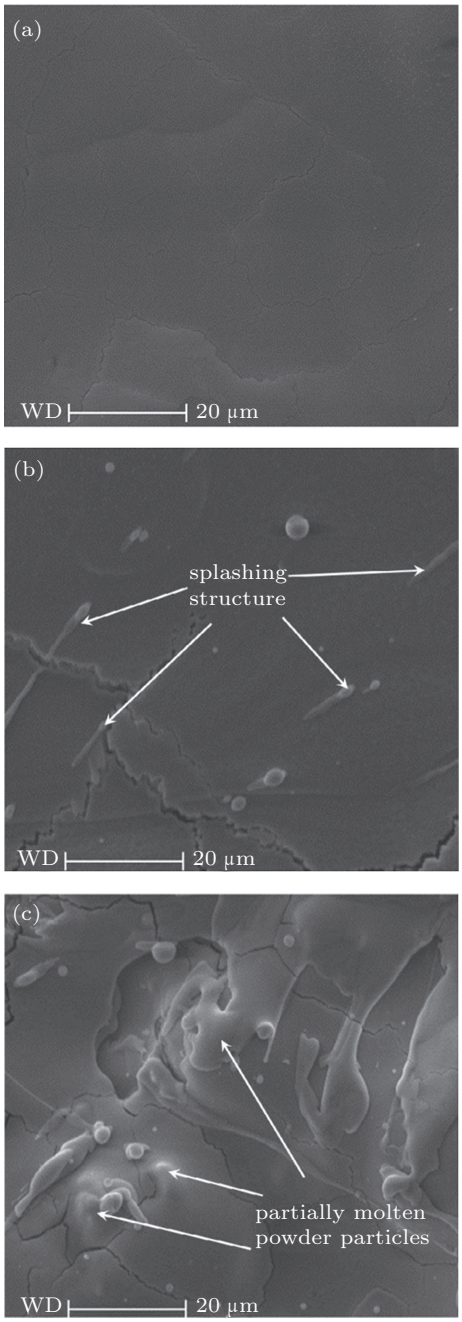


Fig. 18. (a) SEM views of the zirconia coating surface prepared in the laminar jet, (b) in transitional jet, and (c) in turbulent jet.

4. Conclusions

In this study, the characteristics of helium plasma jets generated in a DC plasma torch with multiple cathodes are experimentally investigated. The jet parameters, including length, voltage fluctuation, thermal efficiency, specific enthalpy, temperature, etc., are measured. Furthermore, the applications of the device for the preparation of zirconia coatings are tested under different flow states of the plasma jet. The following conclusions are drawn from this study:

(i) As the gas flow rate increases, the plasma jet transforms from the laminar state to the transitional state and then to the turbulent state. Compared with the transitional/turbulent jets, the laminar jet has better stability and a longer high-temperature zone. The increasing arc currents not only help to improve the jet's length but also help to increase the critical flow rate for the generation of a laminar jet.

(ii) The arc voltage and thermal efficiency increase with the addition of the gas flow rate. On the other hand, the specific enthalpy decreases with the increase in the gas flow rate. It is inferred that the increase in the gas flow rate surpasses the effect of the total enthalpy on the specific enthalpy.

(iii) As the gas flow rate increases, the core temperature at the nozzle's outlet decreases but the core velocity increases significantly. Additionally, with the change of jet states from the laminar flow to the turbulent flow, the decaying rates of the jet's temperature, gage pressure, and velocity increase rapidly along the jet's axial direction. This phenomenon is thought to stem from the intensified air entrainment in the transitional /turbulent jet.

(iv) By using the central axis to send the powder, the zirconia coating is prepared under different flow states of the plasma jet. The results indicate that the long laminar jet is favorable for the deposition of a high-quality coating during the spraying procedure. It is concluded that the powder particles in the laminar jet may provide lower kinetic energy and better heating. These two factors can limit the splashing of particle droplets and ensure the effective melting of the powder particles.

References

[1] Mostaghimi J and Boulos M I 2015 *Plasma Chemistry and Plasma Processing* **35** 421
[2] Solonenko O P, Nishiyama H, Smirnov A V, Takana H and Jang J 2015 *Journal of Visualization* **18** 1
[3] Winter J, Brandenburg R and Weltmann K D 2015 *Plasma Sources Science & Technology* **24** 064001
[4] Pfender E 1994 *Thin Solid Films* **238** 228
[5] Miao J G, Yu D P, Cao X Q, Xiang Y, Xiao M and Yao J 2015 *Plasma Chemistry and Plasma Processing* **35** 879
[6] Pan W X, Zhang W H, Zhang W H and Wu C K 2001 *Plasma Chemistry and Plasma Processing* **21** 23
[7] Pan W X, Zhang W H, Ma W and Wu C K 2002 *Plasma Chemistry and Plasma Processing* **22** 271
[8] Pan W X, Li G, Meng X, Ma W and Wu C K 2005 *Pure Appl. Chem.* **77** 373
[9] Cheng K, Xu D Y, Meng X, Chen X and Pan W 2006 *Pure Appl. Chem.* **78** 1253
[10] Pan W, Meng X, Wu C and Chen X 2006 *Plasma Chemistry and Plasma Processing* **26** 335

[11] Cheng K, Chen X and Pan W 2006 *Plasma Chemistry and Plasma Processing* **26** 211
[12] Wang H X, Chen X, Cheng K and Pan W X 2007 *Int. J. Heat Mass Transfer* **50** 734
[13] Wang H X, Xi C and Pan W 2007 *Plasma Chemistry and Plasma Processing* **27** 141
[14] Pan W X, Meng X, Li G, Fei Q X and Wu C K 2005 *Surface & Coatings Technology* **197** 345
[15] Guang-Zhi, U. W, Teng L I and Pan W X 2006 *Heat Treatment of Metals* **31** 143
[16] Ma W, Fei Q, Pan W and Wu C 2006 *Appl. Surf. Sci.* **252** 3541
[17] Vilotijevic M, Markovic P, Zec S, Marinkovic S and Jokanovic V 2011 *Journal of Materials Processing Technology* **211** 996
[18] Cao X, Yu D, Xiao M, Miao J, Xiang Y and Yao J 2016 *Plasma Chemistry and Plasma Processing* **36** 693
[19] Wang C, Cui H C, Li W W, Liao M R, Xia W L and Xia W D 2017 *Chin. Phys. B* **26** 025202
[20] Wang C, Zhang Z L, Xia W L, Cui H C and Xia W D 2017 *Plasma Chemistry and Plasma Processing* **37** 371
[21] Wang C, Cui H C, Zhang Z L, Xia W L and Xia W D 2017 *Contributions to Plasma Physics* **57** 58
[22] Xiuquan C, Deping Y, Yong X, Jin Y and Jianguo M 2016 *Plasma Sci. Technol.* **18** 740
[23] Osaki K, Fukumasa O and Kobayashi A 2000 *Vacuum* **59** 47
[24] Fauchais P and Vardelle A 2000 *Int. J. Thermal Sci.* **39** 852